Technical Report: Targeted Proteomic Analysis Reveals Enrichment of Atypical Ubiquitin Chains in Contractile Murine Tissues

Tiaan Heunis[1,2], Frederic Lamoliatte[1,2], José Luis Marín-Rubio[1], Abeer Dannora[1] and Matthias Trost[1]*

[1]Biosciences Institute, Newcastle University, Newcastle upon Tyne, NE2 4HH, United Kingdom.

[2]These authors contributed equally to this work

*Corresponding author:

Matthias Trost, Tel: +44 191 2087009, E-mail: matthias.trost@ncl.ac.uk

Summary

Ubiquitylation is an elaborate post-translational modification involved in all biological processes. Its pleotropic effect is driven by the ability to form complex polyubiquitin chain architectures that can influence biological functions. In this study, we optimised sample preparation and chromatographic separation of Ubiquitin peptides for Absolute Quantification by Parallel Reaction Monitoring (Ub-AQUA-PRM). Using this refined Ub-AQUA-PRM assay, we were able to quantify all ubiquitin chain types in 10-minute LC-MS/MS runs. We used this method to determine the ubiquitin chain-linkage composition in murine bone marrow-derived macrophages and different mouse tissues. We could show tissue-specific differences in ubiquitin levels in murine tissues, with polyubiquitin chain types contributing a small proportion to the total pool of ubiquitin. Interestingly, we observed enrichment of atypical (K33) ubiquitin chains in heart and muscle. Our approach enabled high-throughput screening of ubiquitin chain-linkage composition in different murine tissues and highlighted a possible role for atypical ubiquitylation in contractile tissues.

Main Text

Ubiquitylation is a post-translational modification that results from the addition of ubiquitin, a 76 amino acid protein, to generally the ε-amino group of a lysine residue. Ubiquitylation plays a role in practically all eukaryotic biological processes. It is therefore not surprising that aberrant

ubiquitylation is linked to several human diseases, including cancer, infectious, neurodegenerative, and developmental diseases [1]. Protein substrates can be modified by monoubiquitin or can be polyubiquitylated, which is formed by further ubiquitylation of any lysine (K6, K11, K27, K29, K33, K48, and K63) or the N-terminal methionine (M1) of ubiquitin. This allows formation of complex chain architectures (homotypic, heterotypic, or branched chains), which can ultimately influence a substrates fate [2]. However, the biological functions of atypical and mixed ubiquitin chains are only beginning to emerge [1,3]. Therefore, methods are needed to rapidly screen the ubiquitin chain-linkage landscape in cells and tissues to advance our understanding of ubiquitin signalling, especially for atypical linkage types as there are few tools available that facilitate their analysis [4]. Recent technological advances in mass spectrometry-based proteomics have enabled quantification of endogenous levels of ubiquitin chain types by selected reaction monitoring (Ub-AQUA-SRM) [5]. This approach has subsequently been adapted to quadrupole-Orbitrap instruments using parallel reaction monitoring (PRM) [6] to determine chain-linkage composition of purified substrates [7], whole-cell lysates [8], to quantify K48-K63 branched chains [9,10], to gain information on higher-order chain-linkage architecture of ubiquitylated substrates [7] and to quantify phosphorylated and acetylated ubiquitin [11,12]. Here we further refined the Ub-AQUA-PRM method for absolute quantification of ubiquitin chain types. We optimised peptide oxidation, ion-pairing agents, and implemented microflow chromatographic separation for increased assay sensitivity and throughput. Our refined Ub-AQUA-PRM assay is ideal for high-throughput screening of ubiquitin chain types in diverse samples, as demonstrated here using murine primary cells and tissues.

Methionine-containing peptides can be challenging to analyse by PRM-based methods, as they can occur in different oxidation states [13]. This can become problematic for quantification when the peptide signal is divided across multiple oxidation states or, importantly, when there are differences between the endogenous peptide and the spike-in standard. Current Ub-AQUA-PRM strategies analyse the methionine sulfoxide version of methionine-containing peptides, induced by using low concentrations of H_2O_2 at 4°C [13,14]. However, these peptides are stable for only 21.5 hours, before oxidation state shifts are observed [13]. We therefore fully oxidised methionine residues into the sulfone derivative using H_2O_2. No difference in methionine sulfone-containing peptide (M1 or K6) intensity was observed without H_2O_2 at room temperature or 60°C for 2 hours (Supplementary Figure 1a, b). However, a methionine sulfone was generated when using 0.1% H_2O_2 at 60°C for 2 hours, but the sulfoxide version still contributed substantially to M1 and K6 peptide intensity. Both methionine-containing peptides (M1 and K6) were converted into a stable methionine sulfone by more than 99.9%, based on peptide intensity, when using 1% H_2O_2 for 2 hours at 60°C (Supplementary Figure S1a, b). The other peptides analysed were unaffected under the same

64 conditions (Supplementary Figure S1c). This indicates that our oxidation procedure does not
65 introduce undesirable artifacts. We, therefore, used 1% H_2O_2 for 2 hours at 60°C for peptide
66 oxidation in all further analyses. Next, we determined the optimal normalised collision energy (NCE)
67 required for fragmenting each peptide. Detailed information on NCE used for each peptide is
68 available in Supplementary Table S1. Additionally, we also tested the effect of two commonly used
69 ion-pairing agents in reversed-phase chromatography for their effect on peptide retention and ion
70 intensity, namely formic acid (FA) and trifluoroacetic acid (TFA). We compared FA and TFA at
71 concentrations ranging from 0.2 to 5.0% (v:v) in the loading buffer (Supplementary Figure S2). For all
72 these injections, buffer A and B remained the same. The K29 peptide is the most hydrophilic of the
73 ubiquitin peptides, but we did not observe a major difference in peak intensity or peak shape
74 between 5.0% FA and 0.2% TFA for this peptide (Supplementary Figure S2a). However, we observed
75 a marked decrease in intensity for other ubiquitin peptides when using TFA, even as low as 0.2%
76 (Supplementary Figure S2b). We, therefore, used 5.0% FA in the sample buffer for all further
77 analyses. Finally, we determined the lower limit of detection (LLOD) and lower limit of quantification
78 (LLOQ) of each peptide in a simple (ubiquitin peptides only) and complex (*E. coli* tryptic digest)
79 matrix. We opted for an *E. coli* tryptic digested as spike-in matrix as no endogenous ubiquitin is
80 present in this organism that would interfere with the assay. LLOD for peptides were as low as 0.5
81 amol on column. In the simple matrix we could achieve LLOQ ranging from 50 amol for the M1 and
82 K29 peptides to 1.5 fmol for the K11, K63 and TITTITLEVEPSDTIENVK ubiquitin peptides. Similar
83 results were obtained for ubiquitin peptides in the complex matrix (Supplementary Figure S3),
84 reaching LLOQ as low as 0.1 fmol/µg protein injected. These results indicate that our refined Ub-
85 AQUA-PRM assay could accurately quantify low levels of endogenous ubiquitin chain types in
86 complex matrixes.

87 We used our Ub-AQUA-PRM assay to screen the ubiquitin chain-linkage composition in
88 primary murine macrophages (BMDMs), given the importance of ubiquitin in innate immunity [15–
89 18]. Additionally, we validated our Ub-AQUA-PRM assay using MG132, a proteasome inhibitor that
90 results in ubiquitin accumulation, especially K48 chains [19,20]. An increase in the percentage of
91 polyubiquitin chains was observed in BMDMs after treatment with MG132, as would be expected
92 (Figure 1a, b). All linkage types could be detected in murine BMDMs with K48 (63.2%), K63 (24.2%)
93 and K29 (8.0%) contributing 95.4% of the total ubiquitin chain-linkage composition of whole-cell
94 lysates (Figure 1c). These results are in agreement with previous reports in cell lines [7,21]. Similarly,
95 K48 (71.8%), K63 (15.5%) and K29 (5.2%) contributed 92.5% of the total ubiquitin chain-linkage
96 composition of BMDMs during MG132 treatment (Figure 1c). Next, we determined whether there
97 was any difference in ubiquitin chain types during treatment with MG132 for 6 hours. We observed

98 a statistically significant increase in the majority of ubiquitin chain types, including total ubiquitin,
99 during MG132 treatment (Supplementary Figure S4), which is in agreement with previous reports
100 [7,19,22]. However, K11 and K27 chain types were below the limit of quantification during our
101 analysis. These results indicate that K48, K63 and K29 linkage types dominate the ubiquitin chain-
102 linkage compositions in murine BMDM whole-cell lysates and that up to ~29.2% of total ubiquitin is
103 in the polyubiquitylated form in resting BMDMs.

104 Lastly, we used our Ub-AQUA-PRM assay to screen the ubiquitin chain-linkage composition
105 of six different murine tissues (brain, heart, kidney, lung, muscle, and spleen) from three different
106 mice. We were able to detect ubiquitin in all samples, with the brain, kidney, and spleen having the
107 highest levels of total ubiquitin (Supplementary Figure S5). A statistically significant difference in
108 total ubiquitin was observed in the brain, which had higher levels of total ubiquitin than the heart,
109 lung, and muscle (Supplementary Figure S5). Interestingly, only a small percentage of total ubiquitin
110 seems to be polyubiquitylated in murine tissues, with the contribution of chain types to total
111 ubiquitin being ~1% in most tissues (Figure 2a). The lung had ~1.4% of total ubiquitin in the
112 polyubiquitylated form, whereas muscle had the highest with ~8.7%. In most tissues, K48 was the
113 most dominant chain type (Figure 2b), similar to what we observed in BMDMs. However, we
114 observed differences in ubiquitin chain-linkage composition in heart and muscle. Interestingly, K33
115 was enriched in heart and muscle, compared to the other tissues (Figure 2b). In order to determine
116 the percentage contribution of the K33 linkage type to the total pool of ubiquitin, we normalised this
117 chain type to total ubiquitin in each tissue. K33 contributed only a small proportion to the total pool
118 of ubiquitin, with 5.3 ± 1.9% in muscle and 3.0 ± 1.3% in heart. We verified that these results were
119 not an artefact of our experimental procedure by using a different extraction buffer before Ub-
120 AQUA-PRM analysis. We observed similar results in muscle when using TCA extraction buffer in an
121 independent experiment, with K33 contributing to 5.7 ± 0.9% of the total pool of ubiquitin.
122 Noteworthy, we observed a slightly lower contribution of K33 to the total ubiquitin chain-linkage
123 composition when using TCA extraction, but K33 still contributed >56% to the total ubiquitin chain-
124 linkage composition in muscle (Supplementary Figure S6). This discrepancy is likely due to the
125 different extraction buffer used, which could affect the protein composition extracted from the
126 tissues.

127 These results indicate that there are tissue-specific differences in total ubiquitin and
128 ubiquitin chain types in murine tissues, with atypical linkages increased in heart and muscle.
129 Furthermore, our data indicate that only a small proportion of total ubiquitin in murine tissues are in
130 the polyubiquitin form. It is, therefore, possible that many proteins in murine tissues are either
131 monoubiquitylated, or that the majority of ubiquitin is in its unconjugated, free form. To test this,

132 we performed immunoblots for total ubiquitin (conjugated and unconjugated) using the same
133 tissues analysed by Ub-AQUA-PRM. We observed high levels of unconjugated ubiquitin in the
134 majority of tissues (Supplementary Figure S7). However, we did observe conjugated ubiquitin in all
135 tissues. More unconjugated ubiquitin was observed in the brain, kidney, lung, and spleen, whereas
136 heart and muscle had the least amount of unconjugated ubiquitin. In our Ub-AQUA-PRM assay, we
137 also observed lower levels of total ubiquitin in the heart and muscle, which corresponds to the data
138 obtained with the western blots. This data indicates that there are major tissue-specific differences
139 in ubiquitylation and that only a small proportion of total ubiquitin in murine tissues are in the
140 conjugated form. Further analysis of the ubiquitylome and ubiquitin chain-linkage landscape, in
141 combination with recently described methods such as Ub-clipping [21] and Ubiquitin Chain
142 Enrichment Middle-Down Mass Spectrometry (UbiChEM-MS) [23], could reveal detailed information
143 on atypical ubiquitylation and higher-order chain-linkage architecture in different tissues and
144 pathological states.

145

146 **Methods – online methods**

147 *Preparation of AQUA peptides*

148 Synthetic ubiquitin peptides were obtained from Cambridge Research Biochemicals (Cleveland,
149 United Kingdom) (Supplementary Table S1). Methionine-containing peptides were synthesised under
150 their reduced form, and were subsequently oxidised during sample preparation, as described below.
151 Peptides were dissolved at a concentration of 1 nmol/µl in 50:50 acetonitrile:water (v:v) and peptide
152 purity was monitored by LC-MS/MS. Peptides lacking net peptide content were injected together
153 with their isotope counterpart and net peptide content was determined based on the ratio between
154 the two isotopes. Two sets of master mixes were prepared, with the 10 light and 10 heavy peptides
155 mixed, separately, in equimolar concentrations. The light and heavy peptide master mixes were
156 diluted, separately, to 10 pmol/µl in HPLC-grade water (Thermo Fisher Scientific) and stored at -
157 80°C.

158

159 *Optimization of methionine oxidation and ion-pairing agents for targeted proteomic analysis of*
160 *Ubiquitin AQUA peptides*

161 Methionine oxidation was optimised to generate a stable methionine sulfone for targeted proteomic
162 analysis. Heavy and light peptides were mixed in a 1:1 ratio and incubated with different
163 concentrations of H_2O_2 at either room temperature (RT) or 60°C. The conversion of reduced

164 methionine to sulfoxide and sulfone derivatives were monitored by LC-MS/MS. The effect of ion-
165 pairing agents on peptide retention and intensity was assessed by using increasing concentrations of
166 formic acid (FA) and trifluoracetic acid (TFA) in the sample and loading buffers, as indicated in the
167 text.

168

169 *Preparation of standard curves*

170 The heavy master mix was diluted to 100 fmol/µl and the light master mix was serially diluted from
171 10 pmol/µl to 1 amol/µl using a dilution factor of √10. The standard curve was prepared on ice by
172 combining reaction components in the following order: 20 µl of HPLC-grade water, 10 µl of heavy
173 mix at 100 fmol/µl, 10 µl of light mix at varying concentrations, 50 µl of 10% FA, and 10 µl of 10%
174 H_2O_2. A second standard curve was prepared by substituting 10 µl of HPLC-grade water with 10 µl of
175 *Escherichia coli* tryptic digest at 1 µg/µl. The *E. coli* tryptic digest was generated as described below.
176 Samples were incubated for 2h at 60°C for oxidation, before targeted proteomic analysis.

177

178 *Bacterial cell culture for proteomic analysis*

179 *E. coli* DH5-α was cultured overnight in Luria-Bertani (Thermo Fisher Scientific) broth at 37°C with
180 shaking at 180 rpm. The next day, cells were harvested (4,000 xg, 15 min, 4°C), washed twice with
181 ice-cold PBS pH 7.4 and stored at -80°C until further analysis. Cell pellets were lysed in 5% SDS in 50
182 mM triethylammonium bicarbonate (TEAB) pH 7.5, by sonication. Whole-cell lysates were
183 subsequently centrifuged (10,000 xg, 5 min, RT) and the supernatants used for proteomic sample
184 preparation.

185

186 *Murine cell culture and tissue collection*

187 Animal work was approved by the Newcastle University ethical committee and performed under UK
188 Home Office project licence (PCI 23A338). Bone marrow-derived macrophages (BMDMs) were
189 derived from femurs of 8 to 12-week-old C57BL/6 mice. Bone marrow was extracted and
190 differentiated into macrophages using Iscove's Modified Dulbecco's Media (IMDM; Sigma-Aldrich)
191 supplemented with 10% heat-inactivated foetal calf serum (Thermo Fisher Scientific), 1% L-
192 glutamine (Lonza), 1% penicillin/streptomycin (Lonza) and 20% L929-conditioned media for 7 days at
193 37 °C in 5% CO_2 humidified atmosphere. After differentiation, BMDMs were stimulated with 10 µM
194 MG132 (Sigma-Aldrich) for 6 hours or mock treated. After stimulation, BMDMs were washed twice

195 with ice-cold PBS pH 7.4. Cells were subsequently lysed by sonication in 5% SDS in 50 mM TEAB pH
196 7.5, supplemented with 100 mM N-ethylmaleimide (NEM, Sigma-Aldrich) to inhibit deubiquitylases.
197 Whole-cell lysates were used for proteomic sample preparation.

198 Tissues (brain, heart, lung, kidney, muscle and spleen) were collected from 8 to 12-week-old
199 C57BL/6J mice, washed once with ice-cold PBS pH 7.4, flash frozen in liquid nitrogen and stored at -
200 80°C until further analysis. Tissues were ground to a powder in liquid nitrogen using a mortar and
201 pestle, and lysed by sonication in lysis buffer (5% SDS in 50 mM TEAB pH 7.5) supplemented with
202 100 mM NEM. Tissue lysates were subsequently centrifuged (10,000 xg, 5 min, RT) and the
203 supernatants used for methanol chloroform precipitation. Protein pellets were resuspended in lysis
204 buffer and used for proteomic sample preparation. In a separate experiment, muscle samples were
205 ground to a powder in liquid nitrogen using a mortar and pestle, and proteins extracted in 20%
206 trichloroacetic acid (TCA) at 4°C. Samples were centrifuged (10,000 xg, 10 min, RT) and washed twice
207 with ice-cold acetone to remove remaining TCA. Protein precipitates were subsequently
208 resuspended in lysis buffer, containing 100 mM NEM, centrifuged to remove debris, and processed
209 as described below.

210

211 *Proteomics sample preparation*

212 Protein concentration for all samples was determined using the bicinchoninic acid assay (BCA) assay
213 (Thermo Fisher Scientific). Fifty µg of total protein was used for proteomics sample preparation by
214 suspension trapping (S-Trap) [24,25], with minor modifications to that recommended by the supplier
215 (ProtiFi, Huntington NY, USA). Samples were reduced with 5 mM tris(2-carboxyethyl)phosphine
216 (Pierce) for 15 min at 37°C, and subsequently alkylated with 10 mM NEM for 15 min at room
217 temperature in the dark. Five µl of 12% phosphoric acid was added to each sample after reduction
218 and alkylation, followed by the addition of 330 µl S-Trap binding buffer (90% methanol in 100 mM
219 TEAB pH 7.1). Acidified samples were added, separately, to S-Trap mini-spin columns and
220 centrifuged at 4,000 xg for 1 minute. Each S-Trap mini-spin column was washed with 400 µl S-Trap
221 binding buffer and centrifuged at 4,000 xg for 1 minute. This process was repeated for five washes.
222 Twenty-five µl of 50 mM TEAB pH 8.0 containing sequencing-grade trypsin (1:10 ratio of
223 trypsin:protein) was added to each sample, followed by proteolysis for 2 hours at 47°C using a
224 thermomixer (Eppendorf). Peptides were eluted with 50 mM TEAB pH 8.0 and centrifugation at
225 1,000 xg for 1 minute. Elution steps were repeated using 0.2% FA and 0.2% FA in 50% acetonitrile,
226 respectively. The three eluates from each sample were combined and dried using a speed-vac before
227 storage at -80°C. Peptides were subsequently reconstituted to 1 µg/µl using 5% FA in water and

228 prepared for PRM, on ice, by combining reagents in the following order: 30 µl of HPLC-grade water,
229 10 µl peptide digest at 1 µg/µl, 10 µl of heavy master mix at 100 fmol/µl, 40 µl of 10% FA and 10 µl
230 of 10% H_2O_2. Samples were incubated for 2h at 60°C for oxidation before targeted mass
231 spectrometry analysis.

232

233 *Targeted LC-MS/MS analysis - Parallel Reaction Monitoring (PRM)*

234 Peptide samples were injected on a Dionex Ultimate 3000 RSLC (Thermo Fisher Scientific) connected
235 to a Q-Exactive HF mass spectrometer (Thermo Fisher Scientific). Fifty fmol of each ubiquitin peptide
236 was injected during analysis, along with 500 ng of tryptic peptide mixture from either *E. coli* or *Mus*
237 *musculus* as indicated in the text. In order to minimise dead volume and shorten the analysis to only
238 10 min, we used a direct injection LC setup. During the loading phase, samples are loaded using a 5
239 µl loop and full loop injection, with a 2.4 µl needle and an overfill ratio of 1.5. Samples were injected
240 onto a 150 µm x 150 mm EASY-Spray LC column (Thermo Fisher Scientific) using the nano-pump and
241 100% buffer A (96.9% HPLC-grade water, 3% DMSO, 0.1% FA) at 1.5 µl/min. After 4 min (6 µl), the
242 column oven valve was switched to bypass the loop and peptides were eluted by increased
243 concentration of buffer B (80% HPLC-grade acetonitrile, 16.9% HPLC-grade water, 3% DMSO, 0.1%
244 FA) using a multistep gradient (Supplementary Table S2). The source was heated to 320°C and 2.5 kV
245 was applied between the column emitter and the MS. The Q-Exactive HF was operated in PRM mode
246 using a resolution of 15,000, AGC target of 2×10^5 and maximum injection time of 25 ms. Peptides
247 were selected for MS/MS data acquisition using pre-determined isolation windows and fragmented
248 using collision energies described in Supplementary Table S1.

249

250 *Targeted proteomic data analysis*

251 All Ub-AQUA-PRM RAW mass spectrometry files were analysed using Skyline-daily (version
252 4.1.1.11871) [26]. Fragment ion intensities were extracted and light to heavy (L/H) ratios of peptide
253 pairs were automatically determined in Skyline. All extracted ion chromatograms were manually
254 inspected. Standard curves were generated from log transformed L/H ratios and peptide
255 concentrations, to determine the lower limit of detection (LLOD) and lower limit of quantification
256 (LLOQ) for each peptide. The R^2 was determined based on the LLOQ of each peptide. Only curves
257 with a R^2 value > 0.99 were used for determining the absolute concentration of total ubiquitin and
258 the different ubiquitin chain types. Group comparisons were performed using a Student's t-test, and
259 multiple group comparisons were performed using an analysis of variance (ANOVA), followed by a

Tukey's HSD test for determining significance for pairwise comparisons, in GraphPad Prism (version 8.0.1). The mass spectrometry proteomics data have been deposited to the ProteomeXchange [27] Consortium via the PRIDE [28] partner repository with the dataset identifier PXD017754. Reviewers can access it through the Username: reviewer39102@ebi.ac.uk and the password vJ56s8uk.

Western blots

Total protein from brain, heart, kidney, lung, muscle and spleen were extracted as described above. Ten-microgram protein from each sample were separated on 12% SDS-PAGE gels before being electrotransferred to Immobilon-P transfer membranes (Merck Millipore). Membranes were probed with monoclonal antibody for mono-and polyubiquitylated proteins (FK2)(BML-PW8810; Enzo Life Sciences), anti-α-Tubulin (T9026; Sigma-Aldrich) and anti-Histone H3 (D1H2) (4499; Cell Signaling) antibodies. Corresponding secondary antibodies used included anti-mouse IgM, HRP-conjugated (AP307P; Sigma-Aldrich) and anti-rabbit IgG, HRP-conjugated (7074; Cell Signaling Technology) antibodies. Peroxidase activity was developed using the Amersham™ ECL™ Prime Western Blotting Detection Reagent (GE Healthcare) and imaged on an Amersham Imager 600 digital imaging system (GE Healthcare). To assess equal loading of protein, Ponceau staining (Sigma-Aldrich) of the PVDF membranes was performed.

Acknowledgements

This work was funded by a Wellcome Trust Investigator Award (215542/Z/19/Z) and the generous start-up funding of Newcastle University to MT. FL was funded by a Marie Skłodowska-Curie Fellowship from the Horizon 2020 programme of the EU (project number 795670).

Conflict of interest

The authors declare no conflict of interest.

Author contributions

TH, FL and MT designed the study. TH and FL performed mass spectrometry experiments and data analysis. JLM-R performed western blots. AD was responsible for animal husbandry and animal experimental procedures. TH and MT wrote the paper with contribution of all authors.

290

291 **References**

292 [1] H.J. Meyer, M. Rape, Enhanced protein degradation by branched ubiquitin chains, Cell. 157
293 (2014) 910–921. https://doi.org/10.1016/j.cell.2014.03.037.

294 [2] K.N. Swatek, D. Komander, Ubiquitin modifications, Cell Res. 26 (2016) 399–422.
295 https://doi.org/10.1038/cr.2016.39.

296 [3] C.N. Cunningham, J.M. Baughman, L. Phu, J.S. Tea, C. Yu, M. Coons, D.S. Kirkpatrick, B. Bingol,
297 J.E. Corn, USP30 and parkin homeostatically regulate atypical ubiquitin chains on
298 mitochondria, Nat. Cell Biol. 17 (2015) 160–169. https://doi.org/10.1038/ncb3097.

299 [4] R.E. Heap, M.S. Gant, F. Lamoliatte, J. Peltier, M. Trost, Mass spectrometry techniques for
300 studying the ubiquitin system, Biochem. Soc. Trans. 45 (2017) 1137–1148.
301 https://doi.org/10.1042/BST20170091.

302 [5] D.S. Kirkpatrick, N.A. Hathaway, J. Hanna, S. Elsasser, J. Rush, D. Finley, R.W. King, S.P. Gygi,
303 Quantitative analysis of in vitro ubiquitinated cyclin B1 reveals complex chain topology, Nat.
304 Cell Biol. 8 (2006) 700–710. https://doi.org/10.1038/ncb1436.

305 [6] H. Tsuchiya, K. Tanaka, Y. Saeki, The parallel reaction monitoring method contributes to a
306 highly sensitive polyubiquitin chain quantification, Biochem. Biophys. Res. Commun. 436
307 (2013) 223–229. https://doi.org/10.1016/j.bbrc.2013.05.080.

308 [7] H. Tsuchiya, D. Burana, F. Ohtake, N. Arai, A. Kaiho, M. Komada, K. Tanaka, Y. Saeki, Ub-ProT
309 reveals global length and composition of protein ubiquitylation in cells, Nat. Commun. 9
310 (2018). https://doi.org/10.1038/s41467-018-02869-x.

311 [8] T.P. Miettinen, J. Peltier, A. Härtlova, M. Gierliński, V.M. Jansen, M. Trost, M. Björklund,
312 Thermal proteome profiling of breast cancer cells reveals proteasomal activation by CDK 4/6
313 inhibitor palbociclib, EMBO J. 37 (2018) 1–19. https://doi.org/10.15252/embj.201798359.

314 [9] F. Ohtake, Y. Saeki, S. Ishido, J. Kanno, K. Tanaka, The K48-K63 branched ubiquitin chain
315 regulates NF-κB signaling, Mol. Cell. 64 (2016) 251–266.
316 https://doi.org/10.1016/j.molcel.2016.09.014.

317 [10] F. Ohtake, H. Tsuchiya, Y. Saeki, K. Tanaka, K63 ubiquitylation triggers proteasomal
318 degradation by seeding branched ubiquitin chains, Proc. Natl. Acad. Sci. 115 (2018) E1401–
319 E1408. https://doi.org/10.1073/PNAS.1716673115.

320 [11] F. Koyano, K. Okatsu, H. Kosako, Y. Tamura, E. Go, M. Kimura, Y. Kimura, H. Tsuchiya, H.
321 Yoshihara, T. Hirokawa, T. Endo, E.A. Fon, J.F. Trempe, Y. Saeki, K. Tanaka, N. Matsuda,
322 Ubiquitin is phosphorylated by PINK1 to activate parkin, Nature. 510 (2014) 162–166.
323 https://doi.org/10.1038/nature13392.

324 [12] F. Ohtake, Y. Saeki, K. Sakamoto, K. Ohtake, H. Nishikawa, H. Tsuchiya, T. Ohta, K. Tanaka, J.
325 Kanno, Ubiquitin acetylation inhibits polyubiquitin chain elongation, EMBO Rep. 16 (2015)
326 192–201. https://doi.org/10.15252/embr.201439152.

327 [13] L. Phu, A. Izrael-Tomasevic, M.L. Matsumoto, D. Bustos, J.N. Dynek, A. V. Fedorova, C.E.
328 Bakalarski, D. Arnott, K. Deshayes, V.M. Dixit, R.F. Kelley, D. Vucic, D.S. Kirkpatrick, Improved
329 quantitative mass spectrometry methods for characterizing complex ubiquitin signals, Mol.
330 Cell. Proteomics. 10 (2011) 1–19. https://doi.org/10.1074/mcp.M110.003756.

331 [14] H. Tsuchiya, K. Tanaka, Y. Saeki, The parallel reaction monitoring method contributes to a
332 highly sensitive polyubiquitin chain quantification, Biochem. Biophys. Res. Commun. (2013).
333 https://doi.org/10.1016/j.bbrc.2013.05.080.

334 [15] L. Deng, C. Wang, E. Spencer, L. Yang, A. Braun, J. You, C. Slaughter, C. Pickart, Z.J. Chen,
335 Activation of the Iκb kinase complex by TRAF6 requires a dimeric ubiquitin-conjugating
336 enzyme complex and a unique polyubiquitin chain, Cell. (2000).
337 https://doi.org/10.1016/S0092-8674(00)00126-4.

338 [16] F. Tokunaga, S.I. Sakata, Y. Saeki, Y. Satomi, T. Kirisako, K. Kamei, T. Nakagawa, M. Kato, S.
339 Murata, S. Yamaoka, M. Yamamoto, S. Akira, T. Takao, K. Tanaka, K. Iwai, Involvement of
340 linear polyubiquitylation of NEMO in NF-κB activation, Nat. Cell Biol. 11 (2009) 123–132.
341 https://doi.org/10.1038/ncb1821.

342 [17] B. Gerlach, S.M. Cordier, A.C. Schmukle, C.H. Emmerich, E. Rieser, T.L. Haas, A.I. Webb, J.A.
343 Rickard, H. Anderton, W.W.L. Wong, U. Nachbur, L. Gangoda, U. Warnken, A.W. Purcell, J.
344 Silke, H. Walczak, Linear ubiquitination prevents inflammation and regulates immune
345 signalling, Nature. 471 (2011) 591–596. https://doi.org/10.1038/nature09816.

346 [18] M.U. Gack, Y.C. Shin, C.H. Joo, T. Urano, C. Liang, L. Sun, O. Takeuchi, S. Akira, Z. Chen, S.
347 Inoue, J.U. Jung, TRIM25 RING-finger E3 ubiquitin ligase is essential for RIG-I-mediated
348 antiviral activity, Nature. 446 (2007) 916–920. https://doi.org/10.1038/nature05732.

349 [19] F. Ohtake, H. Tsuchiya, Y. Saeki, K. Tanaka, K63 ubiquitylation triggers proteasomal
350 degradation by seeding branched ubiquitin chains, Proc. Natl. Acad. Sci. U. S. A. 115 (2018)

351 E1401–E1408. https://doi.org/10.1073/pnas.1716673115.

352 [20] K.L. Rock, C. Gramm, L. Rothstein, K. Clark, R. Stein, L. Dick, D. Hwang, A.L. Goldberg,
353 Inhibitors of the proteasome block the degradation of most cell proteins and the generation
354 of peptides presented on MHC class I molecules, Cell. (1994). https://doi.org/10.1016/S0092-
355 8674(94)90462-6.

356 [21] K.N. Swatek, J.L. Usher, A.F. Kueck, C. Gladkova, T.E.T. Mevissen, J.N. Pruneda, T. Skern, D.
357 Komander, Insights into ubiquitin chain architecture using Ub-clipping, Nature. (2019).
358 https://doi.org/10.1038/s41586-019-1482-y.

359 [22] H. Tsuchiya, F. Ohtake, N. Arai, A. Kaiho, S. Yasuda, K. Tanaka, Y. Saeki, In vivo ubiquitin
360 linkage-type analysis reveals that the Cdc48-Rad23/Dsk2 axis contributes to K48-linked chain
361 Ssecificity of the proteasome, Mol. Cell. 66 (2017) 488-502.e7.
362 https://doi.org/10.1016/j.molcel.2017.04.024.

363 [23] S.O. Crowe, A.S.J.B. Rana, K.K. Deol, Y. Ge, E.R. Strieter, Ubiquitin chain enrichment middle-
364 down mass spectrometry enables characterization of branched ubiquitin chains in cellulo,
365 Anal. Chem. 89 (2017) 4428–4434. https://doi.org/10.1021/acs.analchem.6b03675.

366 [24] A. Zougman, P.J. Selby, R.E. Banks, Suspension trapping (STrap) sample preparation method
367 for bottom-up proteomics analysis, Proteomics. 14 (2014) 1006–1010.
368 https://doi.org/10.1002/pmic.201300553.

369 [25] M. HaileMariam, R.V. Eguez, H. Singh, S. Bekele, G. Ameni, R. Pieper, Y. Yu, S-Trap, an
370 ultrafast sample-preparation approach for shotgun proteomics, J. Proteome Res. 17 (2018)
371 2917–2924. https://doi.org/10.1021/acs.jproteome.8b00505.

372 [26] B. MacLean, D.M. Tomazela, N. Shulman, M. Chambers, G.L. Finney, B. Frewen, R. Kern, D.L.
373 Tabb, D.C. Liebler, M.J. MacCoss, Skyline: An open source document editor for creating and
374 analyzing targeted proteomics experiments, Bioinformatics. 26 (2010) 966–968.
375 https://doi.org/10.1093/bioinformatics/btq054.

376 [27] E.W. Deutsch, A. Csordas, Z. Sun, A. Jarnuczak, Y. Perez-Riverol, T. Ternent, D.S. Campbell, M.
377 Bernal-Llinares, S. Okuda, S. Kawano, R.L. Moritz, J.J. Carver, M. Wang, Y. Ishihama, N.
378 Bandeira, H. Hermjakob, J.A. Vizcaíno, The ProteomeXchange consortium in 2017: Supporting
379 the cultural change in proteomics public data deposition, Nucleic Acids Res. 45 (2017) D1100–
380 D1106. https://doi.org/10.1093/nar/gkw936.

381 [28] Y. Perez-Riverol, A. Csordas, J. Bai, M. Bernal-Llinares, S. Hewapathirana, D.J. Kundu, A.

Inuganti, J. Griss, G. Mayer, M. Eisenacher, E. Pérez, J. Uszkoreit, J. Pfeuffer, T. Sachsenberg, Ş. Yilmaz, S. Tiwary, J. Cox, E. Audain, M. Walzer, A.F. Jarnuczak, T. Ternent, A. Brazma, J.A. Vizcaíno, The PRIDE database and related tools and resources in 2019: Improving support for quantification data, Nucleic Acids Res. 47 (2019) D442–D450. https://doi.org/10.1093/nar/gky1106.

Figure legends

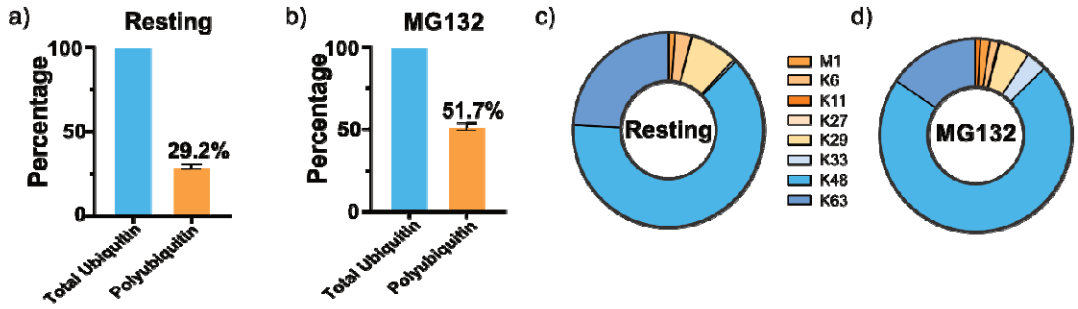

Figure 1. All eight polyubiquitin chain types are present in murine bone marrow-derived macrophages. Percentage of polyubiquitin chain types present in resting, unstimulated (a) and MG132-treated (b) bone marrow-derived macrophages, compared to the total pool of ubiquitin. Contribution of each of the eight different ubiquitin chain types to the total pool of polyubiquitin in resting, unstimulated (c) and MG132-treated bone marrow-derived macrophages (d). Error bars indicate standard deviation.

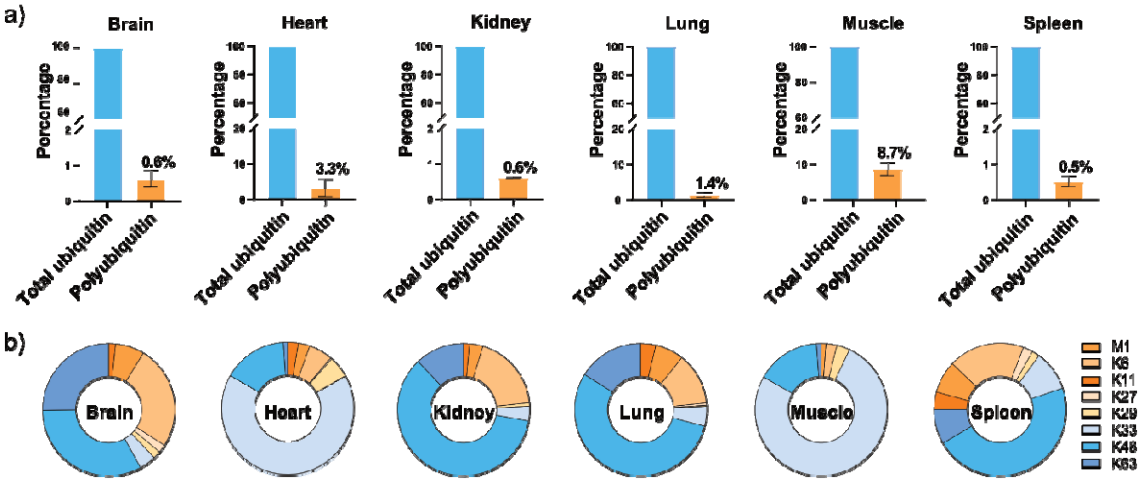

Figure 2. Tissue-specific differences in ubiquitin chain types and compositions exist in murine tissues. (a) Percentage of polyubiquitin chain types present in different murine tissues, compared to the total pool of ubiquitin present in these tissues. (b) Contribution of each of the eight different

ubiquitin chain types to the total pool of polyubiquitin in different murine tissues. Error bars indicate standard deviation.

Supporting documents

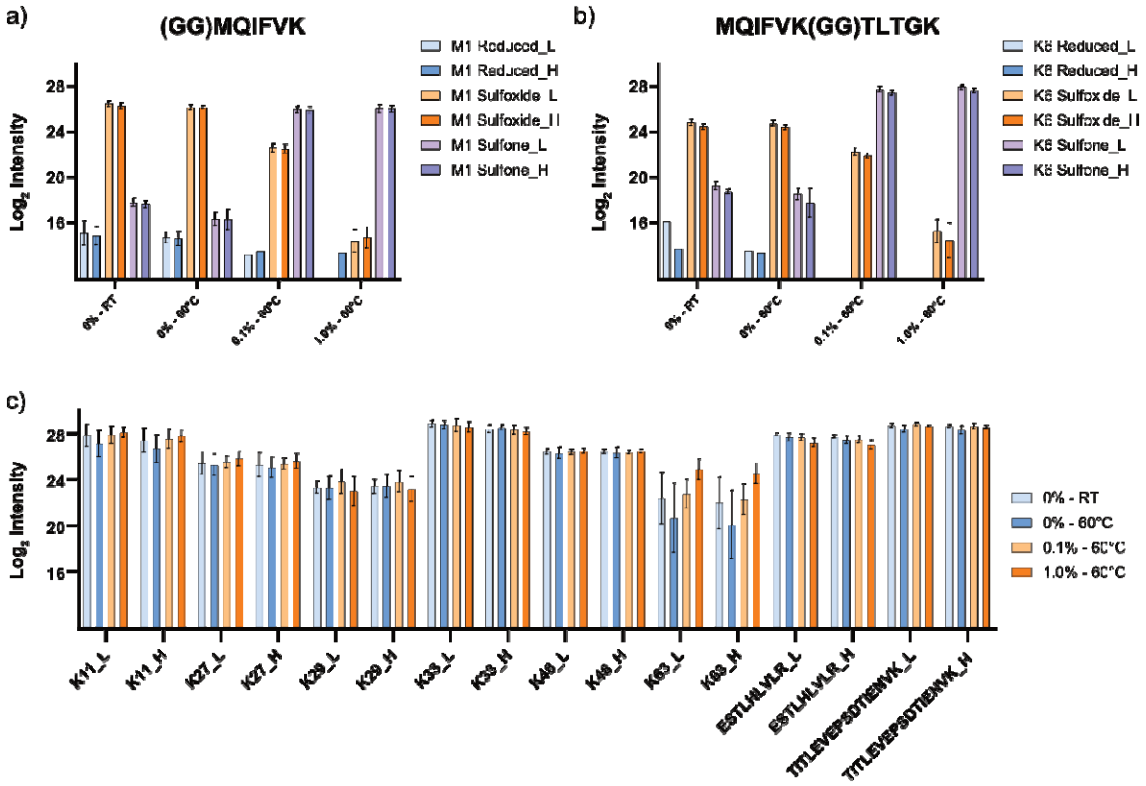

Supplementary Figure S1. Generation of a stable methionine sulfone by oxidation. Methionine-containing ubiquitin peptides were oxidised using hydrogen peroxide (H_2O_2) and analysed by LC-MS/MS to determine the generation of a methionine sulfone. A stable methionine sulfone was generated using 1.0% H_2O_2 at 60°C for 2 hours in M1 (a) and K6 (b) peptides. (c) Peptide intensities observed for non-methionine-containing ubiquitin peptides when using H_2O_2 for oxidation. L = light version of the peptide, H = heavy version of the peptide, LoD = limit of detection. Error bars indicate standard deviation.

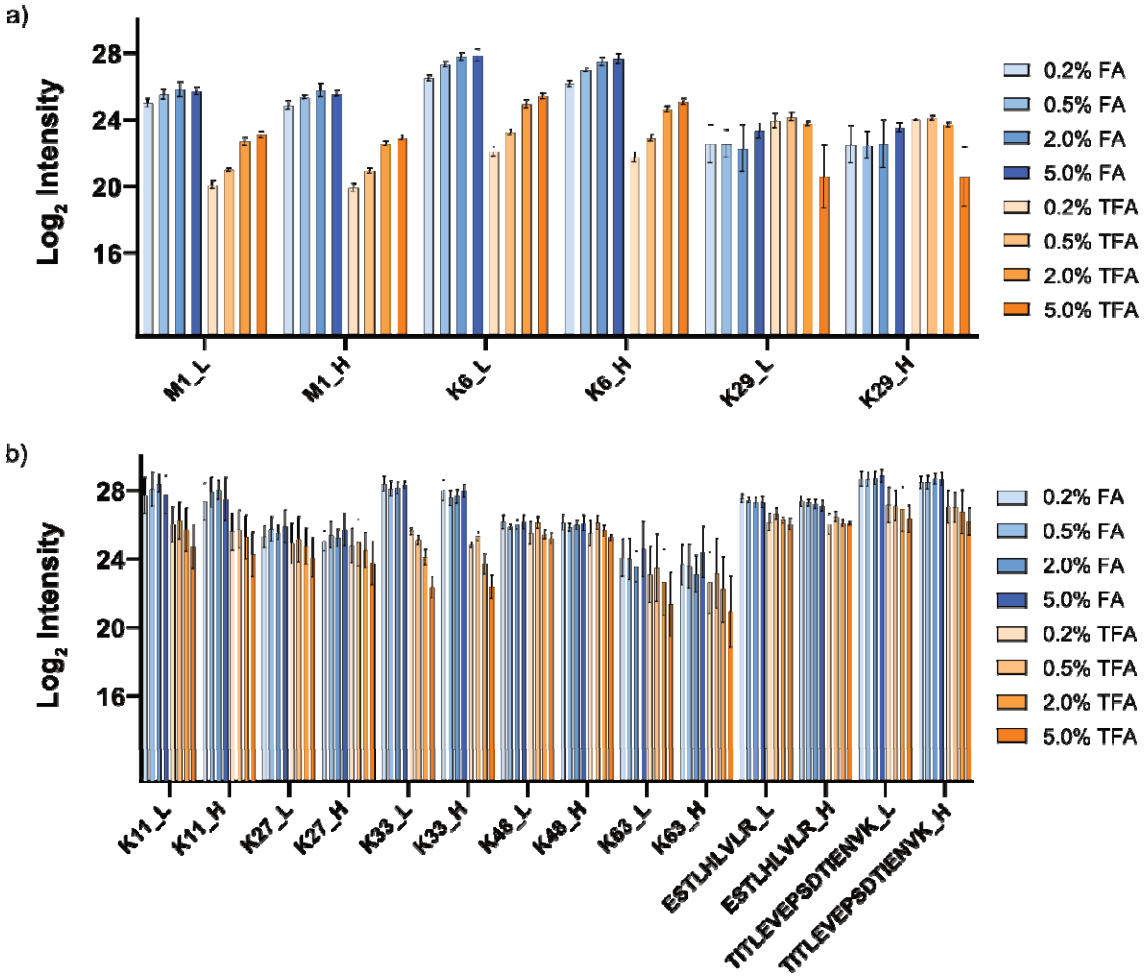

Supplementary Figure S2. Formic acid is a superior ion-pairing agent for ubiquitin peptides. (a) Peptide intensities observed for M1, K6 and K29 ubiquitin peptides when using formic acid (FA) and trifluoroacetic acid (TFA) as ion-pairing agent in the loading buffer. (b) Peptide intensities observed for the other ubiquitin peptides when using FA and TFA in the loading buffer. L = light version of the peptide, H = heavy version of the peptide, LoD = limit of detection. Error bars indicate standard deviation.

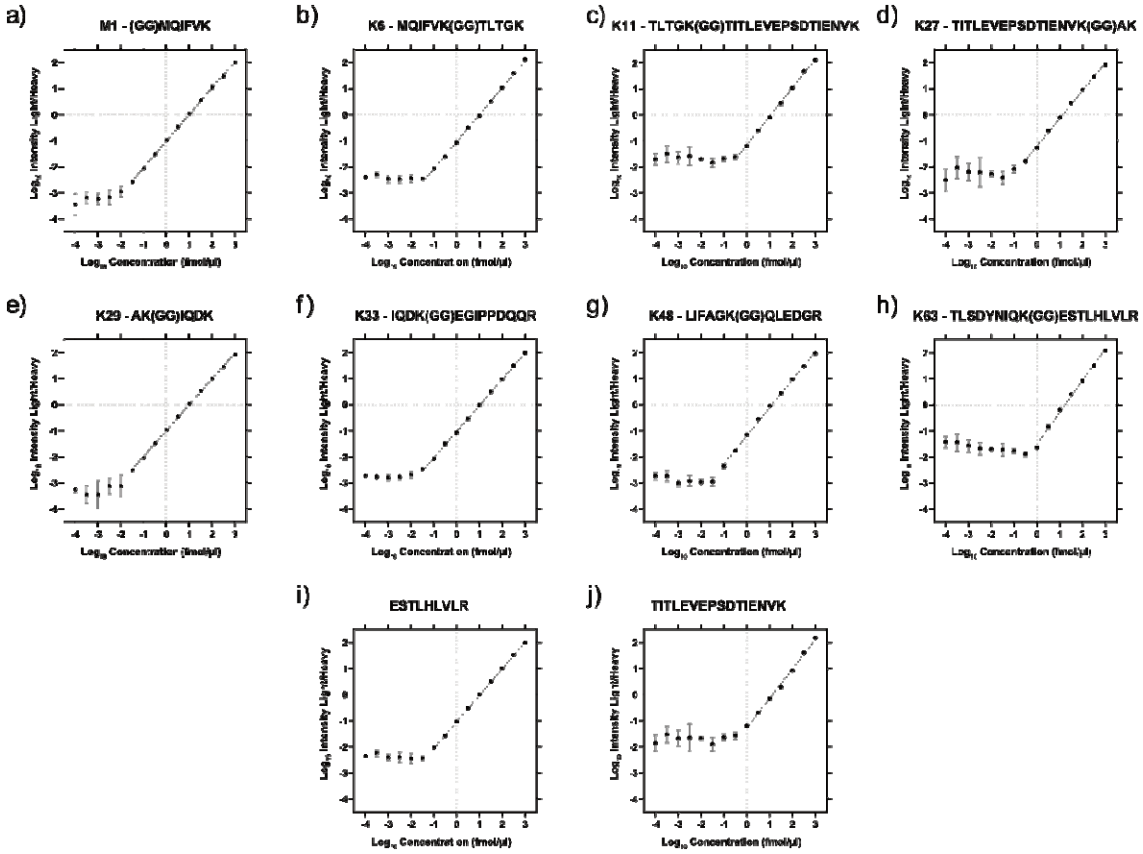

Supplementary Figure S3. Limits of detection and quantification of spiked-in, heavy and light ubiquitin peptides in an *E. coli* proteome digest. Standard curves were generated using 10 synthetic ubiquitin peptides in their light and heavy counterparts. Heavy peptides were used at 10 fmol/µl, while light peptides were serially diluted from 1 pmol/µl to 1 amol/µl. Peptides were oxidised using H_2O_2 before injected on a Q-Exactive HF mass spectrometer for PRM analysis. The peptide master mix contained each of the eight different ubiquitin chain-type peptides (a-h) and two peptides that served as proxy for total ubiquitin (i, j). Error bars indicate standard deviation.

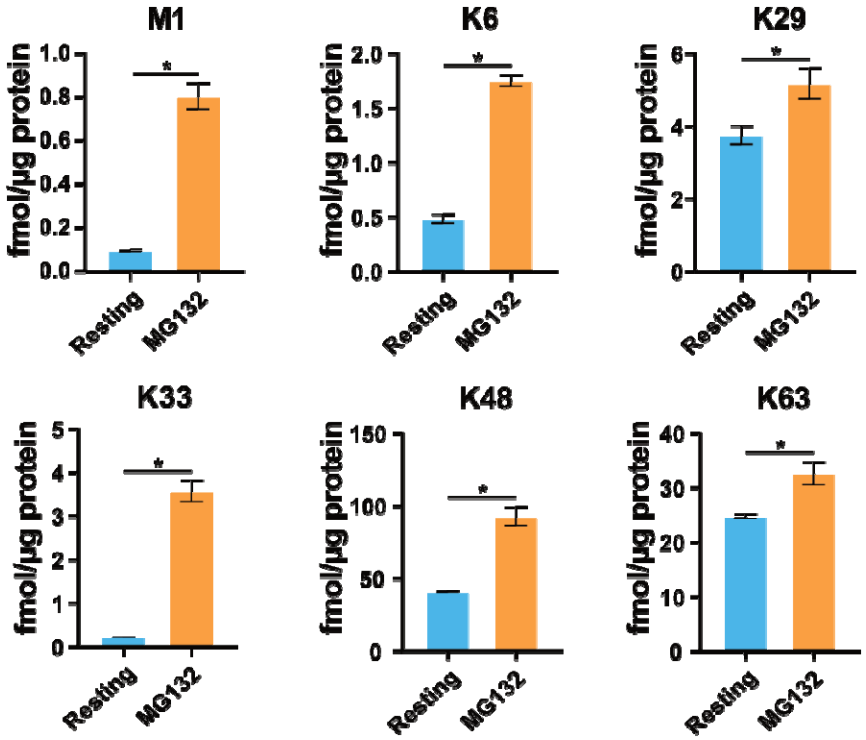

427

428 **Supplementary Figure S4.** MG132 treatment causes an increase in ubiquitin chain types. Differences
429 observed in the quantified ubiquitin chain types at resting state and during MG132 treatment.
430 Statistical significance is denoted with an * and indicates a p-value < 0.05 determined using a
431 Student's t-test. Error bars indicate standard deviation.

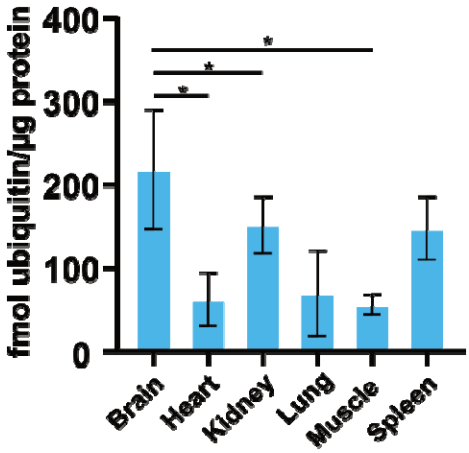

432

433 **Supplementary Figure S5.** Murine tissues contain different levels of ubiquitin. Absolute
434 concentration of ubiquitin in different murine tissues when using non-modified peptides as proxy for
435 total ubiquitin. Total ubiquitin was derived from the sum of the absolute concentrations of
436 TITLEVPSDTIENVK and K11 ubiquitin peptides. Statistical significance is denoted with an * and

437 indicates an adjusted p-value < 0.05 after a Tukey's HSD test and ANOVA. Error bars indicate
438 standard deviation.

439

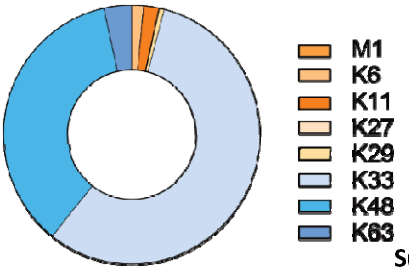

440 **Supplementary Figure S6.** Mouse muscle is enriched in K33
441 ubiquitin chain types. (a) Contribution of each of the eight different ubiquitin chain types to the total
442 pool of polyubiquitin in mouse muscle when using 20% TCA for protein extraction to inhibit
443 deubiquitylase activity.

444

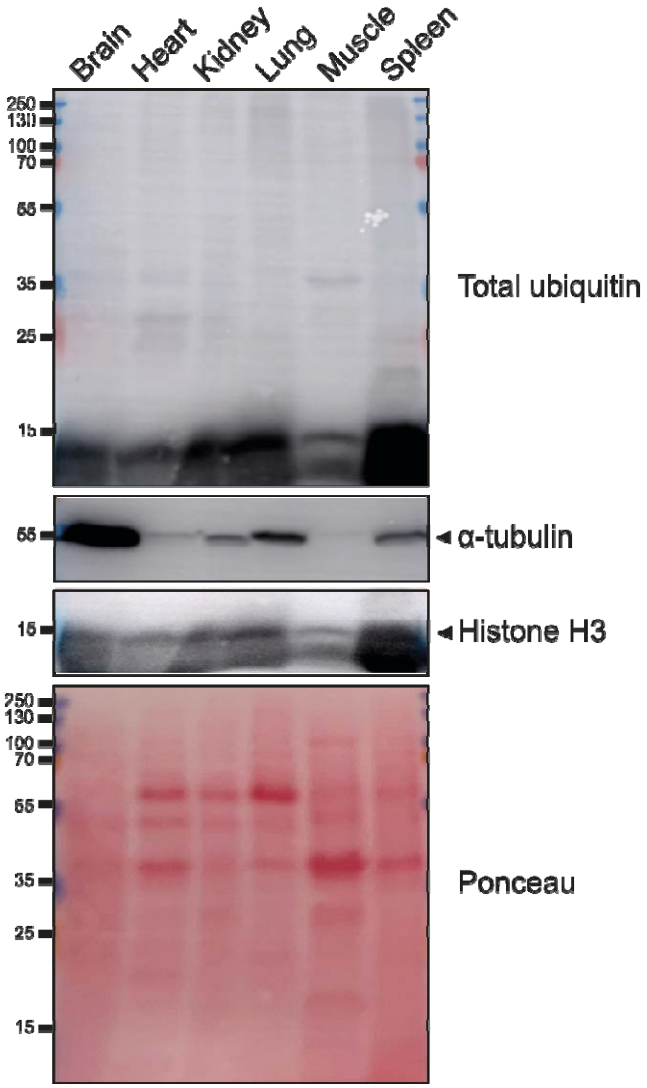

Supplementary Figure S7. Murine tissues contain a large amount of unconjugated ubiquitin. Western blot for total ubiquitin (conjugated and unconjugated) in murine tissues. The same tissues were used as those analysed by Ub-AQUA-PRM.

Supplementary Table S1. Peptides used for absolute quantification of ubiquitin chain types by Ub-AQUA-PRM analysis.

Supplementary Table S2. Multi-step gradient used for separating ubiquitin peptides during Ub-AQUA-PRM analysis.

456

457

458

459 **Supplementary Table S1.** Peptides used for absolute quantification of ubiquitin chain types by Ub-
460 AQUA-PRM analysis.

Sequence	m/z	Z	RT (min)	NCE (%)	Transitions
GGM(ox^2)QIFVK[$^{13}C_6{}^{15}N_2$]	460.2435	2+	6.7	20	y3$^+$, y5$^+$, y6$^+$, y4$^+$, y2$^+$
GGM(ox^2)QIFVK	456.2364	2+	6.7	20	y3$^+$, y5$^+$, y6$^+$, y4$^+$, y2$^+$
M(ox^2)QIFVK(**GG**)TLTGK[$^{13}C_6{}^{15}N_2$]	710.3914	2+	7.2	24	y8$^+$, y6$^+$, y9$^+$, y7$^+$, y5$^+$
M(ox^2)QIFVK(**GG**)TLTGK	706.3843	2+	7.2	24	y8$^+$, y9$^+$, y6$^+$, y7$^+$, y5$^+$
TLTGK(**GG**)TITLEVEPSDTIENVK[$^{13}C_6{}^{15}N_2$]	804.0983	3+	9.3	20	y9$^+$, y9^{2+}, y10$^+$, y19^{2+}, y11$^+$
TLTGK(**GG**)TITLEVEPSDTIENVK	801.4269	3+	9.3	20	y9$^+$, y9^{2+}, y10$^+$, y19^{2+}, y11$^+$
TITLEVEPSDTIENVK(**GG**)AK[$^{13}C_6{}^{15}N_2$]	1055.061	2+	9	22	y11$^+$, y12$^+$, y13$^+$, y3$^+$, y14$^+$
TITLEVEPSDTIENVK(**GG**)AK	1051.054	2+	9	22	y11$^+$, y12$^+$, y13$^+$, y3$^+$, y14$^+$
AK(**GG**)IQDK[$^{13}C_6{}^{15}N_2$]	412.7394	2+	5.7	26	y4$^+$, y2$^+$, y3$^+$, y5$^+$, y5^{2+}
AK(**GG**)IQDK	408.7323	2+	5.7	26	y4$^+$, y2$^+$, y3$^+$, y5$^+$, y5^{2+}
IQDK(**GG**)EGIPP[$^{13}C_5{}^{15}N$]DQQR[$^{13}C_6{}^{15}N_4$]	551.9536	3+	6.3	22	y6^{2+}, y6$^+$, y5$^+$, y5^{2+}, y3$^+$
IQDK(**GG**)EGIPPDQQR	546.6129	3+	6.3	22	y6^{2+}, y6$^+$, y5$^+$, y5^{2+}, y3$^+$
LIFAGK(**GG**)QLEDGR[$^{13}C_6{}^{15}N_4$]	735.9006	2+	7.3	24	y8$^+$, y10$^+$, y10^{2+}, y9$^+$, y2$^+$
LIFAGK(**GG**)QLEDGR	730.8964	2+	7.3	24	y8$^+$, y10$^+$, y10^{2+}, y9$^+$, y2$^+$
TLSDYNIQK(**GG**)ESTLHLVLR[$^{13}C_6{}^{15}N_4$]	752.0737	3+	9.2	20	y16^{2+}, y13^{2+}, y15^{2+}, y14^{2+}, y11^{2+}
TLSDYNIQK(**GG**)ESTLHLVLR	748.7376	3+	9.2	20	y16^{2+}, y13^{2+}, y15^{2+}, y14^{2+}, y11^{2+}
ESTESTLHLVLR[$^{13}C_6{}^{15}N_4$]	539.3182	2+	7.2	28	y5$^+$, y4$^+$, y3$^+$, y5^{2+}, y6$^+$
ESTESTLHLVLR	534.314	2+	7.2	28	y5$^+$, y4$^+$, y3$^+$, y5^{2+}, y6$^+$
TITTITLEVEPSDTIENVK[$^{13}C_6{}^{15}N_2$]	898.4744	2+	9.5	20	y9$^+$, y10$^+$, y11$^+$, y12$^+$, y14$^+$

TITTITLEVEPSDTIENVK	894.4673	2+	9.5	20	$y9^+$, $y10^+$, $y11^+$, $y12^+$, $y14^+$

461 *Ox^2 = sulfone version of methionine

462

463

464 **Supplementary Table S2.** Multi-step gradient used for separating ubiquitin peptides during Ub-
465 AQUA-PRM analysis.

Time (min)	%B
0	0
4	0
4.25	7
5	12
6	15
7	16
8	24
8.25	35
8.5	90
8.75	90
9	0
10	0

466